SAND2018-3668C

ICLASS 2018, 14th Triennial International Conference on Liquid Atomization and Spray Systems, Chicago, IL, July 22-26, 2018

Transient cavitation in transparent diesel injectors

J. Manin[1,2*], L. M. Pickett[1], K. Yasutomi[1,3]

[1] Sandia National Laboratories, 7011 East Ave, 94550 Livermore, CA

[2] Artium Technologies, 470 Lakeside Dr., Sunnyvale, CA

[3] Hino Motors Ltd., Hino-shi, Tokyo, Japan

Abstract

The flow and cavitation behavior inside fuel injectors is known to affect spray development, mixing and combustion characteristics. While diesel fuel injectors with converging and hydro-eroded holes are generally known to limit cavitation and feature higher discharge coefficients during the steady period of injection, less is known about the flow during transients of needle opening and closing. Multiple injection strategies involve short injections, multiplying the transients and giving them a growing importance as part of the fuel delivery process. In this study, single-hole transparent nozzles were manufactured with the same hole inlet radius and diameter as the Engine Combustion Network Spray D nozzle, mounted to a modified version of a common-rail Spray A injector body and needle. The transients of needle opening and closing were visualized with stereoscopic high-speed microscopy at injection pressures relevant to modern diesel engines. Time-resolved sac pressure was extracted via elastic deformation analysis of the transparent nozzles. Sources of cavitation were observed and tracked, enabling the identification of a gas exchange process after the end of injection with ingestion of chamber gas into the sac and orifice. We observed that the gas exchange contributed widely to disrupting the start of injection and outlet flow during the following injection event.

Keywords: Internal flow, Cavitation, Diesel spray, Microscopy.

Introduction

Spray formation and mixing are crucial phenomena for combustion systems. In reciprocating engines, the processes of direct fuel injection into the cylinder is highly transient and closely tied to efficiency and potential for pollutant formation. Although our understanding of high-pressure sprays is progressing, a missing component is the linkage between flows inside the nozzle and the effect on the emerging spray. Several studies have linked internal flow hydraulic characteristics to spray development and mixing [1, 2], through correlation of injection mass flow rate or momentum flux to spray penetration and dispersion. Hydraulic characterization under the appropriate operating conditions is valuable to understand the flow behavior of the injection system and necessary to provide the correct boundary conditions to computational fluid dynamic (CFD) simulations. However, these measurements fail to capture the detailed physics of the phenomena occurring within the injector, namely the inception and development of cavitation, as well as the highly important transient processes.

Quite remarkably, researchers have been able to manufacture transparent fuel injector nozzles with real-size holes, despite typical diameters of only 0.1-0.3 mm, to permit study of internal flow at practical conditions. Prototype nozzles made of various materials such as acrylic or quartz, have permitted the application of optical diagnostics to scrutinize the flow behavior inside micro-orifices. [3, 4, 5, 6, 7, 8, 9, 10, 11, 12, 13, 14]. These studies have made substantial progress in our understanding of hydraulic and cavitation behavior in high-pressure flow and spray processes.

On the other hand, there has been less focus on the transient periods of the injection event in this emerging field. High temporally resolved techniques, with repeatable control, are necessary to capture the fast, transitory processes driving global hydraulic characteristics, spray development and mixing processes. This aspect becomes particularly important in modern diesel engines, where injection strategies rely on multiple injections per cycle. In most cases, quasi-steady quantities are not representative of the flow, as the needle valve moves throughout the entirety of the injection, requiring study of the entire transient process of each injection and of multiple successive injections. With the progress made in high-speed digital imaging, as well as manufacturing techniques, recent studies employed high-speed microscopy to track the evolution of the inside flow and injected spray at relevant injector and ambient operating conditions. Hayashi and coworkers [11] have even used a quartz nozzle featuring three side-located, 0.14-mm orifices injecting into a reacting combustion environment prepared in an optically-accessible rapid compression machine.

Parallel to the experimental efforts, CFD modeling of the internal flow is needed to develop more predictive models of the spray phenomenon. However, one weakness in this area is that the state of the nozzle sac, defined

as the volume between the needle valve and the holes, is often unknown and undefined. This recognition is particularly significant for "DNS-level" volume-of-fluids simulations, where high computational costs limit the simulation time to only the early transient period. Consequently, if boundary conditions are unknown, the relevance and universal conclusions of these simulations is questioned. Microscopic visualization of starting spray from metal fuel injectors at engine conditions already shows evidence of gas injection leading liquid injection [2, 15] with collateral effects on initial flow characteristics and spray development. For example, recent measurements show that once liquid is injected, its initial liquid flow velocity exiting the injector does not ramp up from zero, thus affecting transient rate of injection used in CFD [16].

In this work, we designed real-size optically transparent nozzles matching the Engine Combustion Network (ECN) Spray D geometry (see exact surface geometry at ecn.sandia.gov). A cylindrical, sharp-edged version of the nozzle was also tested to observe the effect of cavitation on the transients. Based upon availability, the nozzles were mounted on a modified ECN Spray A injector. Experiments were performed in an optically-accessible pressure chamber able to emulate pressurized ambient conditions, typical of modern Direct-Injection (DI) diesel engines. We performed stereoscopic high-speed microscopy to visualize the internal flow and cavitation, as well as the near-nozzle spray formation. The remaining of the manuscript is organized as follows. The experimental methods are described, detailing the constant-flow, high-pressure optical chamber, the stereoscopic high-speed imaging arrangement, and the transparent nozzle, including advanced geometry characterization. The results section presents the temporally-resolved needle lift and sac pressurization process, followed by the end of injection gas exchange, leading to the start of injection transients.

Experimental Methods

Pressure vessel

Experiments were conducted using an optically-accessible chamber designed specifically for internal flow visualization and measurements in optically-transparent nozzles, as shown in Fig. 1. The vessel is equipped with four 25-mm diameter fused silica windows, providing dual or stereoscopic line-of-sight optical access to the transparent nozzle. The geometry of the chamber was tailored to allow short working distances and large numerical apertures for microscope imaging to perform optimally. The nozzle is placed on a pedestal with open slots on four sides, allowing direct visualization of the flow exiting the transparent nozzle as well as within the nozzle. The open slots also permit air entrainment into the spray. The orifice is vertically-aligned and a modified ECN Spray A solenoid-actuated injector is mounted atop the transparent nozzle. More details on the nozzle geometries and assemblies are provided in a later section. The chamber operates with N_2 gas at constant-pressure. A flow is typically maintained to scavenge the chamber internal volume, limiting the likelihood of window contamination during repeated spray operation.

n-Dodecane fuel was used in the system for these experiments. The fuel was pressurized by a high-pressure syringe pump, and injection pressure was varied between 25 and 150 MPa, but repeated nozzle failures at 150 MPa convinced us to set the upper injection pressure target to 100 MPa. It should be noted that the fuel was not degassed for these tests, and that a trace amount of air should be expected to dissolve under the conditions kept in the laboratory. Dissolved gas is also expected in regular diesel fuel tanks. The ambient conditions tested in this work ranged from atmospheric to 2.0 MPa, while the temperature was kept constant at 20°C, resulting in a peak ambient density condition of 22.8 kg/m^3, matching the ECN Spray A ambient density.

Imaging diagnostics

A stereoscopic system was developed to acquire detailed high-speed visualizations of the internal flow and near-nozzle spray from optically-transparent nozzles (Fig. 1). Each imaging system was composed of a long-working-distance microscope lens (Infinity K2 or Infinity KV), a high-speed CMOS camera (Phantom v2512 or Photron SA-X2) and a custom-built illumination system. By synchronizing the two systems, the dual-camera arrangement allows simultaneous stereo or three-dimensional visualization of the needle motion, internal flow and spray dynamics. To assist in the description of the systems and to allow the reader to become familiar with the configurations of each system, they have been labeled primary and secondary systems. The primary corresponds to the Phantom v2512 camera, with the Infinity K2 lens, while the secondary system is composed of the Photron SA-X2 and the Infinity KV lens. The microscope objectives were configured to provide magnification levels of 8X for the primary system and 3X for the secondary one, resulting in imaging scale factor of 3.5 and 7 µm/pixel, respectively. The illumination was provided by a custom blue LED source centered on 455 nm (22 nm bandwidth) for the primary system, and a red LED source (620 nm, 19 nm bandwidth) for the secondary arrangement. The LED illumination sources were driven by an ultrafast, high-current driver, capable of producing pulses shorter than 10 ns at megahertz repetition rates. For these experiments, the pulse duration was set to 30 ns for the primary system and 100 ns for the secondary. The primary system operated at frequencies between 120 and 380 kHz, while the secondary system functioned at 270 kHz throughout the experiments. Although the cameras' exposure times

were set to 2 µs and 2.5 µs for the primary and secondary systems, respectively, the illumination pulse durations determined the exposure timescales. The numerical aperture of the system for the primary configuration was 0.15, while it was 0.10 for the secondary system. For both configurations, the diffraction-limited resolutions are less than half a pixel, and as such, do not represent limitations from the optical system.

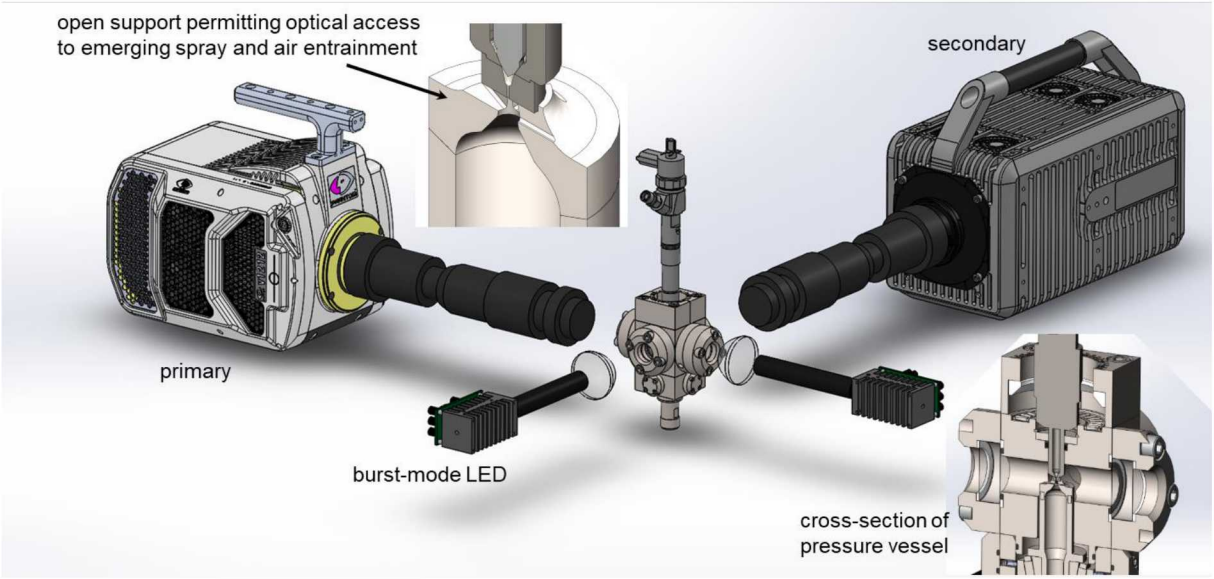

Figure 1 Schematic of the experimental arrangement, showing both high-speed cameras and illumination sources. The pressure vessel is located in the center of the sketch, between the two systems. Insets show details such as the transparent tip support, or a cross-section view of the inside of the chamber.

Transparent nozzle design and geometries

Real-size, optically-transparent nozzles were designed to be mounted at the end of a modified solenoid-actuated ECN Spray A injector. The process is similar to the one described by Liverani et al. [9], where the tip of a production injector nozzle is machined out and replaced by the transparent model. The transparent nozzles were made from cast acrylic, and significant time and effort has been spent to ensure that the nozzle shape was made as specified. Cast acrylic was selected above quartz to avoid brittle material problems, and over sapphire to more closely match the refractive index of the fuel and the nozzle [10]. The ECN Spray D metal nozzle was chosen as the target nozzle. Spray D, is a conical orifice nozzle, with a nominal diameter of 0.186 mm, a k-factor of 1.5 and hydro-grinding was performed to achieve a flow number of 188 g/min with 10 MPa pressure drop. The measured exit nozzle diameter for Spray D is about 0.189 mm. Spray D internal 3-D metal nozzle geometry and hydraulic characterization at realistic diesel injection conditions have been performed by ECN participants and are available to download (ecn.sandia.gov).

The manufactured acrylic nozzles are shown in Fig. 2. The acrylic tips were micro-machined using custom tools for the sac and undersized drills for the hole, and then hydro-eroded to match the flow number of Spray D. Hydro-erosion rounded the inlet and produced an overall geometry that is an excellent match to Spray D, as shown on the left of the figure. The acrylic tips where characterized by microscopic imaging while submerged in a refractive index matching fluid, which showed the most sensitivity for detection of internal surfaces. The measured metal Spray D and Spray A shapes are overlaid on these image for comparison, with an intentional offset second from the left to closely compare the inlet rounding, taper, and hole size. These features of Spray D appear well-represented by the transparent facsimile. The upper regions of the sac are not the same as Spray D, because an extra metal injector with the same dimensions as Spray D was not available at the time. Instead, a Spray A injector was utilized. Since the nozzle was designed to mate and seal with a ground Spray A injector (with support from the bottom and clamping forces from the injector above) as shown in the middle image, the sac (and needle) reflect that of the Spray A injector, which is slightly smaller than the Spray D injector.

The surface roughness of the nozzle was imaged directly with microscopy, but for highest resolution of the surface features, some transparent nozzles were investigated under scanning electron microscopy (SEM) after cutting and gold-coating the specimen. The details seen in the SEM images reveal machining marks and surface textures on the order of 1 µm, which is slightly larger compared to typical hydro-eroded metal injectors, according to past experience from SEM analyses.

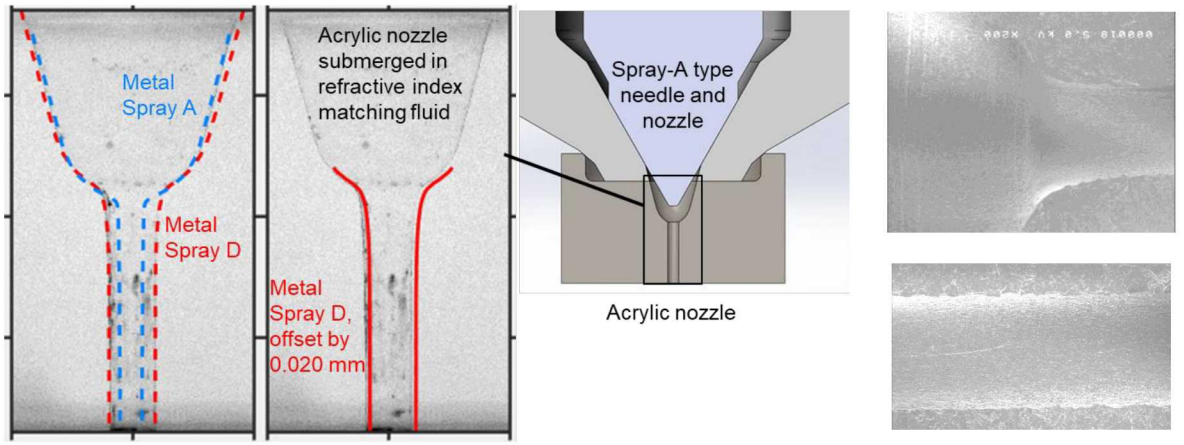

Figure 2 Left: (1) Optical microscopy images of nozzle geometry compared to metal nozzle shapes; (2) Target Spray D shape offset slightly to the right to facilitate comparison to the acrylic wall geometry. Middle: Schematic showing the acrylic tip replacing the metal nozzle mounted on a ground-flat Spray A injector. Right: Geometrical details showing machining marks and other features obtained via SEM imaging of a sectioned tip; the top image illustrates the sac and orifice entrance, while the bottom one shows the region near the orifice exit.

Results and Discussion

Needle-lift and sac pressurization

The tip of the needle can be observed in the sac of the transparent nozzles, thereby offering a direct measurement of needle lift and motion. While needle motion has been reported by other groups, whether via Foucault sensors attached to the rod, or x-ray phase contrast imaging [19], needle motion is system-dependent and such measurements are valuable to understand the impact of needle throttling during opening and closing transients. The needle profile is the result of complex hydraulics initiated as the solenoid is energized, a control volume above the needle is depressurized, and hydraulic force on the other side overcomes the force exerted by the spring keeping the needle closed under non-energized conditions (e.g., see [17]). Visualization within the transparent nozzle permits visualization of this needle movement along with flow and fuel pressure indicators to better understand the transients of opening and closing of the fuel injector. The needle profile as function of time measured during operation at two injection pressures: 50 and 100 MPa is plotted in Fig. 3. The profiles are reported with respect to the time after the start of injection (ASOI), therefore accounting for the hydraulic delay between the start of energizing and the start of injection.

Sac pressure measurements are also shown in the figure. The physical properties of the transparent nozzles, namely the slight elastic deformation of the acrylic nozzles under pressure, allowed correlating the deformation in the sac with pressure as function of time. The sac only deforms by a few micrometers, but the highly-resolved imaging systems could measure the change in sac diameter, treating the measured elastic deformation of the acrylic as an indirect measure of fuel pressure. A calibration for fuel pressure was taken at no sac pressure, and at the time of peak needle lift at different injection pressures, assuming the sac reaches the upstream pressure during the quasi-steady period of long injections. Sac diameter measurements were taken orthogonal to the injector axis at the sac location of the tip of the needle (needle position before energization). It is important to note that these results were extracted with the sac and orifice filled with liquid, and that sac pressurization has been found to be significantly slower when the sac and orifice contain large amounts of gas.

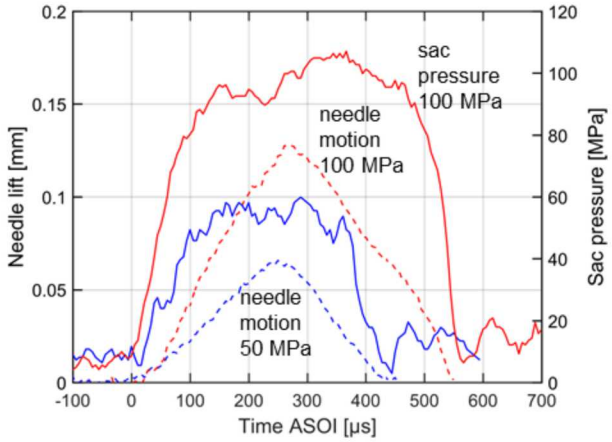

Figure 3 Needle lift (dashed) and estimated sac pressure (solid) profiles as function of time at 50 (blue) and 100 MPa (red) injection pressures. Chamber pressure set to 2.0 MPa.

The needle lift profiles of Fig. 3 show that, as observed by others previously on similar injectors, the lift rate is pressure-dependent, with the 100 MPa injection pressure producing faster lift, approximately twice as fast as the 50 MPa injection pressure. In both cases, the needle rises for over 250 µs, to reach peak lifts on the order of 65 and 125 µm from the initial position, respectively for the 50 and 100 MPa injection pressure cases. We should add that even though energization time was kept constant at 795 µs for both conditions, total injection duration is substantially shorter for 50 MPa compared to 100 MPa, as observed in previous works [17, 18].

By contrast, the measured sac pressure rises and reaches a steady value, and does so much faster than the needle lift. Note that the sac pressure measurement is admittedly sensitive to noise because of the slight sac displacement, but the behavior is still quite clear. For either injection pressure, stable sac pressures are obtained within 100 µs. Note that this behavior is expected if the needle lifts high enough such that the throttling restriction is no longer in the needle-seat area, but within the hole. An analysis of the flow areas at the needle seat compared to the orifice area shows that the needle-seat flow area exceeds the orifice area with only 0.020 mm lift. This requirement is met by 100 µs for either injection pressure. Even though the needle lift is higher at 100 MPa, additional time to pressurize the sac may be expected because of frictional losses through the small-passage seat area and the inertia associated with pressurizing all fluid already in the sac to a higher pressure. The transient rate of depressurization appears to be faster than the pressurization ramp up. The oscillations following the end of injection appear to be real, but the magnitudes of these oscillations are questionable. The end of injection dynamics are discussed in the following section, bringing supporting evidence for pressure oscillations after the needle closes. In summary, the needle lift and sac pressure measurements, obtained together, offer new opportunities to understand injector transient opening and closing effects.

End of injection gas exchange

At first sight, it may seem odd to describe the end of the injection processes before the start of injection. But to establish the conditions that exist within the injector at the beginning of injection, it is important to understand the dynamics and processes occurring at the end of previous injections. The status of the injector sac and holes will change if created by short, multiple injections, or after expansion and compression in an engine. Recent experiments [12, 13, 19] observed that gas bubbles were present in the sac after the end of injection. Mitroglou et al. [12] suggested that these vapor bubbles originate from the end of injection cycle, while Swantek and coworkers [19] hypothesized that the bubbles come from ambient gas, rather than fuel vapor. They found that the presence of gas depends on operating conditions, injection and chamber pressures. At the same time, CFD simulations with different initializations showed that the presence of gas in the sac and orifice affects initial spray development, vaporization rate and liquid penetration [20].

The high-speed movies can help understand the phenomena happening at the end of injection. The high-speed video sequences presented in Video 1 show two examples of an end-of-injection processes. The top sequence corresponds to the end of injection when the injection pressure is set to 50 MPa, and the chamber is set at 2.0 MPa ambient pressure. The bottom sequence features a similar event, but with a chamber pressure set to atmospheric (approximately 0.1 MPa). On these movies, we can observe the transparent injector tip, with the needle inside the sac, located on the left side of the image. The spray exiting the orifice is visible on the right side of the frame. The imaging focus is on the sac, needle, and hole, while the emerging sprays outside of the nozzle are not in focus. Because of the different object planes caused by whether there is or is not acrylic and fuel along the ray path, and the limited depth of field of the microscope setup, one must choose best focus for internal-flow features or the

emerging spray. Fortunately, with our two-camera setup, one camera can be setup for best focus in the sac, and the other for best focus on the spray, if desired. The time reported in the top of the frames is taken with respect to the end of injection, or when the needle closes. No treatment has been applied to these movies, as they come from the raw data acquired by the high-speed camera of the primary system.

The appearance of gas bubbles after the end of injection is clear from the bottom sequence of Video 1. Comparing the low-pressure sequence to the higher chamber pressure condition, where the sac remains filled with liquid fuel, a large amount of gas can be observed in the sac after the injection ends. This low-pressure chamber condition was chosen as an example condition as it enhances the differences and slows down the process such that the phenomena are clearly identified. The low-pressure sequence shows that when the needle closes, some cavitation bubbles move downstream from the needle-seat area, close to the needle, and bubbles are also found in the hole at the same time. A short time later, no bubbles are found in the seat area, but a large phase change occurs in the sac, much larger in size than that of the needle seat area. This phase change occurs in the bulk of the sac, and it does not appear to be connected to fast moving sections of fluid. This "bulk" cavitation process can occur if there is an intense pressure drop throughout all of the fluid, analogous to a fluid-hammer effect in piping systems, where fuel flowing at high-speed, carrying inertia and momentum, is suddenly throttled. For a brief instant, the pressure locally drops below the vapor pressure of the fuel, inducing the fuel to change phase into vapor. The fluid quickly relaxes back to the chamber pressure, thus changing the vaporized fuel back into liquid and collapsing the vapor fuel bubbles. The volume change induced by the collapse rapidly pulls gas from the chamber into the orifice and sac, leaving the orifice and sac with gas from the chamber ambient.

Our observation supports Swantek et al. experiments [19] and Battistoni et al. simulations [20] stating that ambient gas is ultimately ingested into the sac after the end of injection. However, with high-speed visualization, we clarify the underlying mechanism. Cavitation formed in the bulk of the fluid, collapses to ingest gas into the injector. Note that while Battistoni et al. [20] predicted cavitation at similar operating conditions (0.1 MPa ambient pressure) at the end of injection, the cavitation was confined to the needle-seat area, whereas our experiment shows widespread cavitation throughout the bulk of the sac.

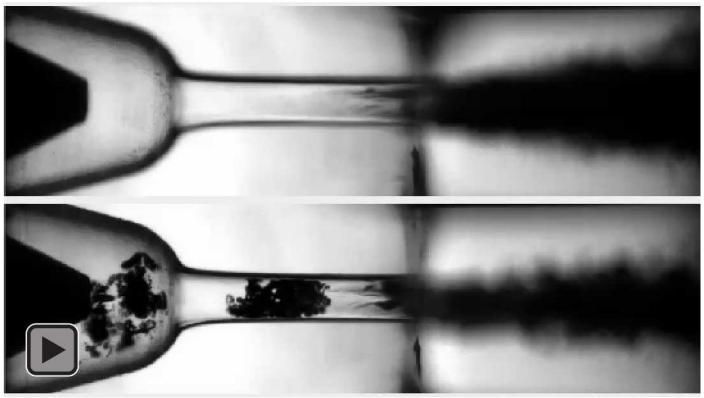

Video 1 Sequences showing the end of injection processes at two chamber conditions. Top: 50 MPa into 2.0 MPa, no gas exchange is observed; Bottom: 50 MPa into 0.1 MPa, shows bulk cavitation and gas exchange.

The gas trapped in the sac most likely is the reason for the fuel dribble observed after the end of injection during the expansion and exhaust phases [21]. The decreasing pressure inside the combustion chamber induces a volumetric expansion of the gas bubbles in the sac, resulting in the left over liquid fuel to be expelled through the orifice(s).

The various experimental conditions tested in this work also correlate with the findings reported by Swantek et al. [19] about the presence or absence of gas bubbles as function of ambient gas pressure. With increasing ambient gas pressure, fewer bubbles are found in the sac—a change more significant than just the expected change in gas volume with increasing pressure. Table 1 summarizes observations made across the different test conditions within our transparent nozzles, which are consistent with Swantek et al. [19].

Table 1 Summary of the observations made over various test conditions regarding bulk cavitation and the presence of gas left over after the end of injection. Columns are ambient pressure and rows are fuel pressure. The tick mark corresponds to a condition where bulk cavitation and gas exchange in the sac is observed, while a cross mark indicates no gas exchange into the sac.

Conditions	0.1 MPa (1 atm.)	0.5 MPa	1.0 MPa	2.0 MPa
25 MPa	✓	✓	×	×
50 MPa	✓	✓	✓	×
100 MPa	✓	✓	✓	✓

The table shows that, in general, higher injection pressure favors bulk cavitation due to a more-intense fluid deceleration at needle closing, resulting in larger amount of gas left over in the sac and orifice. On the other hand, higher ambient pressure reduces the likelihood of cavitation, either in the bulk, or in flow-separation regions within the injector, because the pressure is globally higher within the nozzle, thereby avoiding decreases to the fuel vapor pressure.

As anticipated, the rounded and tapered nozzle does not show signs of significant cavitation at the inlet of the orifice during steady-state operation under the range of conditions tested in this work. Other sharp-edge-inlet nozzles that had no hydro-erosion operation (experiment performed but not shown in this paper), did show signs of cavitation at the inlet, as has been shown in previous work (e.g. [7]).

Start of injection transient

The experiments show that a significant amount of gas can be left over in the sac and orifice after the end of injection, which, as explained earlier, can affect the next injection. The residual gas present in the sac and orifice will be entrained with the liquid flow at the start of the following injection event, as shown numerically by Battistoni et al. [20]. Experiments were performed with different sac status, from almost completely empty to completely full, within what the experiments allow. Video 2 presents two extreme examples, with one injection starting with the sac and orifice nearly full of gas (no liquid), and another similar injection condition, but with the sac and orifice full of liquid (no gas).

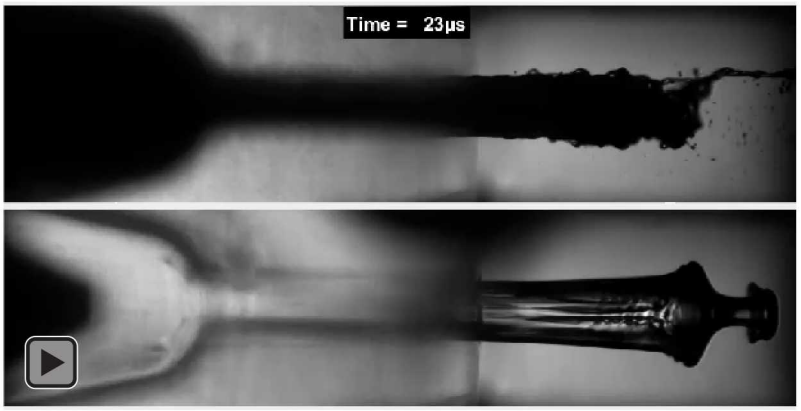

Video 2 Sequences showing the start of injection with different sac status regarding the presence of gas. Top: 25 MPa into 0.1 MPa, sac and orifice full of gas; Bottom: 50 MPa into 0.1 MPa, nozzle full of liquid.

The difference between these two movies is clear at the start of injection. The empty sac and orifice requires a substantial amount of time to fill and mix with gas inside the nozzle. Across the different sac and orifice conditions tested during this campaign, it appeared that the time required for the flow to clear the nozzle of gas depends, as expected, on the quantity of gas initially present in the nozzle. This is indicated by the shadow produced by the gas contained in the sac, as opposed to the relatively clear sac and orifice when filled with fuel. Contrasting with the empty nozzle, the sac and orifice initially full of liquid feature an intact liquid body flowing out of the hole. Spray development, such as initial tip penetration or spray dispersion, also appears to be affected by the initial status of the sac and orifice, whether gas is present or not.

Another interesting aspect of the initially full sac and orifice is that a small amount of gas is pulled from the ambient into the orifice prior to the start of injection. This is attributed to the slight needle lift following the control volume opening [18], producing a volume change significant enough for some gas to enter the orifice. With gas already in the hole, the first liquid flowing out of the orifice already carries momentum as it accelerates through the orifice and exits the nozzle at a non-zero velocity, even initially. An implication of this gas exchange, either from a sac initially or partially full of gas, or from the immediate gas ingestion at the beginning of needle movement, is that the initial rate of injection at the start should not be zero, as suggested by Manin et al. [16]. This result is significant because it is common practice to use rate-of-injection profiles measured in liquid-liquid apparatus that ramp-up from zero.

Detailed microscopic images of the initial flow exiting the orifice also presents interesting features when the nozzle is initially full of liquid. As shown in Fig. 4, geometrical aspects of the flow have been imaged by the high-speed microscopic systems. These sample images show the first 10 – 20 μs after the flow exits the nozzle.

The near-field flow images at the start of injection present smooth geometries and surfaces, as expected with laminar flows, showing noticeable light transmission. With imaging inside the nozzle, which showed ingestion of gas into the hole, we can see that the initial thin section of liquid originates from liquid-gas interfaces formed within the hole, not outside of the hole. Also, features such as the initial mushroom shape of the spray head, surface ripples or thin liquid films and sheets can be observed. The later timings have further time for sac pressurization and velocity increase, as given in the rightmost photographs. The structures in these images are signs that the flow is accelerating, inducing aerodynamic wave oscillations on the flow surface. Subsequent timings not shown in this panel appear highly turbulent, with a typically dark back-illuminated spray, similar to the sprays shown in Video 1. The high-magnitude light attenuation is believed to be the result of the multiple droplets surrounding the core of the sprays, as well as the highly-curved surfaces of the core.

Figure 4 Image sequence showing detailed features of the flow at the start of injection when no gas is present in the nozzle. Injection pressure is 50 MPa, while chamber pressure is 0.1 MPa. The field of view is 1-mm long and images are shown at 10 μs interval.

Summary and Conclusions

Stereoscopic high-speed microscopy was applied to investigate the internal flow details of high-pressure injections. Transparent nozzles were designed based on the well-studied Engine Combustion Network hydro-eroded Spray D. The transparent nozzles were mated to a modified ECN Spray A solenoid-actuated injector, and visualization experiments shown in this manuscript were performed at injection pressures up to 100 MPa. The injector and transparent nozzles were mounted inside an optically-accessible pressure vessel, simulating chamber conditions up to 2.0 MPa in this work. The geometries of the nozzles were investigated in detail via optical microscopy and scanning electron microscopy to ensure that the target nozzle geometries were closely matched.

The temporal information obtained using a two-camera imaging system operating at speeds greater than 100 kHz allowed measurement of the needle motion, internal flow features, and the emerging spray structure. Elastic deformation of the acrylic nozzle was used to compare the needle lift to the sac pressurization process. Beyond the typical cavitation behavior observed in cylindrical nozzles, the temporal information obtained from the different injection events revealed that the end of injection produces a fluid hammer responsible for bulk cavitation of the fluid in the sac under the most realistic conditions. The subsequent collapse of this cavitation fluid ingests gas from the chamber, thus leaving the sac and orifice partly filled with gas. The gas present in the sac affects the following injection, with gas being injected with the liquid fuel for a substantial amount of time.

Acknowledgements

This study was performed at the Combustion Research Facility, Sandia National Laboratories, a multi-mission laboratory managed and operated by National Technology and Engineering Solutions of Sandia, LLC., a wholly owned subsidiary of Honeywell International, Inc., for the U.S. Department of Energy's National Nuclear Security Administration under contract DE-NA0003525. Funding for the project was provided by the Spray Combustion Consortium of automotive industry sponsors, including Convergent Science Inc., Cummins Inc., Ford Motor Co., Hino Motors Ltd., Isuzu Motors Ltd., Groupe Renault, and Toyota Motor Co., with experimental facilities supported by the U.S. DOE Office of Vehicle Technologies.

References

[1] F. Payri, V. Bermúdez, R. Payri, and F. J. Salvador. The influence of cavitation on the internal flow and the spray characteristics in diesel injection nozzles. *Fuel*, 83:419–431, 2004.

[2] L. M. Pickett, J. Manin, R. Payri, M. Bardi, and J. Gimeno. Transient rate of injection effects on spray development. *SAE Paper 2013-24-0001*, 2013.

[3] H. Chaves, M. Knapp, A. Kubitzek, and F. Obermeier. Experimental study of cavitation in the nozzle hole of Diesel injectors using transparent nozzles. *SAE Paper 950290*, 1995.

[4] C. Badock, R. Wirth, and C. Kampmann, S. Tropea. Fundamental study of the influence of cavitation on the internal flow and atomization of Diesel sprays. *ILASS-Europe 1997, Florence, Italy*, pages 53–59, 1997.

[5] N. Tamaki, M. Shimizu, K. Nishida, and H. Hiroyasu. Effects of cavitation and internal flow on atomization of a liquid jet. *Atomization Spray*, 8(2), 1998.

[6] H. Afzal, C. Arcoumanis, M. Gavaises, and N. Kampanis. Internal flow in Diesel injector nozzles: modelling and experiments. *IMechE*, 1999.

[7] M. Blessing, G. Konig, C. Kruger, U. Michels, and V. Schwarz. Analysis of flow and cavitation phenomena in Diesel injection nozzles and its effects on spray and mixture formation. *SAE Paper 2003-01-1358*, 2003.

[8] H. Li and S.H. Collicott. Visualization of cavitation in high-pressure diesel fuel injector orifices. *Atomization Spray*, 16(8):875–886, 2006.

[9] L. Liverani, C. Arcoumanis, H. Yanagihara, i. Sakata, and K. Omae. Imaging of the flow and cavitation formation in a transparent real-size six-hole nozzle under realistic conditions. *The Seventh International Conference on Modeling and Diagnostics for Advanced Engine Systems (COMODIA 2008)*, pages 453–460, 2008.

[10] A. J. Butcher, P. G. Aleiferis, and D. Richardson. Development of a real-size optical injector nozzle for studies of cavitation, spray formation and flash-boiling at conditions relevant to direct-injection spark-ignition engines. *Int. J. Eng. Res.*, 14:557, 2013.

[11] T. Hayashi, M. Suzuki, and M. Ikemoto. Effects of internal flow in a diesel nozzle on spray combustion. *Int. J. Eng. Res.*, 14(6):646–654, 2013.

[12] N. Mitroglou, M. McLorn, M. Gavaises, C. Soteriou, and M. Winterbourne. Instantaneous and ensemble average cavitation structures in diesel micro-channel flow orifices. *Fuel*, 116:736–742, 2014.

[13] M. Winterbourn, C. Soteriou, N. Mitroglou, M. Gavaises, and C. Daveau. Visualising injection events in a fully operational diesel injector with a multi-hole transparent tip. *THIESEL 2014 Conference on Thermo and Fluid-dynamic Processes in Direct Injection Engines, Valencia, Spain*, 2014.

[14] H. Watanabe, M. Nishikori, T. Hayashi, M. Suzuki, N. Kakehashi, and M. Ikemoto. Visualization analysis of relationship between vortex flow and cavitation behavior in diesel nozzle. *Int. J. Eng. Res.*, 16(1):5–12, 2015.

[15] J. Manin, M. Bardi, L. M. Pickett, R. N. Dahms, and J. C. Oefelein. Microscopic investigation of the atomization and mixing processes of diesel sprays injected into high pressure and temperature environments. *Fuel*, 134:531–543, 2014.

[16] J. Manin, M. Bardi, L. M. Pickett, and R. Payri. Boundary condition and fuel composition effects on injection processes of diesel sprays at the microscopic level. *Int. J. Multiphas. Flow*, 83:267–278, 2016.

[17] J. Manin, A. Kastengren, and R. Payri. Understanding the acoustic oscillations observed in the injection rate of a common-rail direct injection diesel injector. *J. Eng. Gas Turb. Power*, 134(12):122801, 2012.

[18] A. Kastengren, Z. Tilocco, and P. Powell. Initial evaluation of engine combustion network injectors with X-Ray diagnostics. *ILASS-Americas 2011, Ventura, CA*, 2011.

[19] A. B. Swantek, D. Duke, F. Z. Tilocco, N. Sovis, C. F. Powell, and A. L. Kastengren. End of injection, mass expulsion behaviors in single hole diesel fuel injectors. *ILASS-Americas 2014, Portland, OR*, 2014.

[20] M. Battistoni, Qi. Xue, and S. Som. Large-eddy simulation (LES) of spray transients: Start and end of injection phenomena. *Oil & Gas Science and Technology*, 71(1), 2016.

[21] W. E. Eagle and M. P. B. Musculus. Cinema-stereo imaging of fuel dribble after the end of injection in an optical heavy-duty diesel engine. *THIESEL 2014 Conference on Thermo and Fluid-dynamic Processes in Direct Injection Engines, Valencia, Spain*, 2014.